Biochemical Journal (2022) **479** 259–272
https://doi.org/10.1042/BCJ20210677

Research Article

TAT–RHIM: a more complex issue than expected

Benedikt Kolbrink[1], Theresa Riebeling[1], Nikolas K. Teiwes[2], Claudia Steinem[2,3], Hubert Kalbacher[4], Ulrich Kunzendorf[1] and Stefan Krautwald[1]

[1]Department of Nephrology and Hypertension, University Hospital Schleswig-Holstein, 24105 Kiel, Germany; [2]Institute of Organic and Biomolecular Chemistry, University of Göttingen, 37077 Göttingen, Germany; [3]Max Planck Institute for Dynamics and Self-Organization, 37077 Göttingen, Germany; [4]Institute of Clinical Anatomy and Cell Analysis, University of Tübingen, Tübingen, Germany

Correspondence: Stefan Krautwald (krautwald@nephro.uni-kiel.de)

Murine cytomegalovirus protein M45 contains a RIP homotypic interaction motif (RHIM) that is sufficient to confer protection of infected cells against necroptotic cell death. Mechanistically, the N-terminal region of M45 drives rapid self-assembly into homo-oligomeric amyloid fibrils, and interacts with the endogenous RHIM domains of receptor-interacting serine/threonine protein kinases (RIPK) 1, RIPK3, Z-DNA-binding protein 1, and Toll/interleukin-1 receptor domain-containing adaptor-inducing interferon-β. Remarkably, all four aforementioned mammalian proteins harbouring such a RHIM domain are key components of inflammatory signalling and regulated cell death (RCD) processes. Immunogenic cell death by regulated necrosis causes extensive tissue damage in a wide range of diseases, including ischaemia reperfusion injury, myocardial infarction, sepsis, stroke, and solid organ transplantation. To harness the cell death suppression properties of M45 protein in a therapeutically usable manner, we developed a synthetic peptide encompassing only the RHIM domain of M45. To trigger delivery of RHIM into target cells, we fused the transactivator protein transduction domain of human immunodeficiency virus 1 to the N-terminus of the peptide. The fused peptide could efficiently penetrate eukaryotic cells, but unexpectedly it eradicated or destroyed all tested cancer cell lines and primary cells irrespective of species without further stimulus through a necrosis-like cell death. Typical inhibitors of different forms of RCD cannot impede this process, which appears to involve a direct disruption of biomembranes. Nevertheless, our finding has potential clinical relevance; reliable induction of a necrotic form of cell death distinct from all known forms of RCD may offer a novel therapeutic approach to combat resistant tumour cells.

Introduction

Regulated cell death (RCD) is an essential part of tissue development, and plays fundamental roles in host defences against pathogens and the maintenance of tissue homeostasis [1]. However, excess activation of RCD pathways can be detrimental and is associated with a wide range of human diseases. Therefore, modulation of RCD and molecules involved in signal transduction cascades has great therapeutic potential for intervention in numerous human diseases including (auto)inflammatory, neurodegenerative, infectious, and metabolic disorders [2].

Necroptosis, the best-described form of regulated necrosis, is characterised by plasma membrane rupture and the release of intracellular contents, which is canonically mediated by a signalling cascade of receptor-interacting serine/threonine protein kinases 1 and 3 (RIPK1/3) and mixed lineage kinase domain-like(MLKL) protein [3]. Three different pathways for activation of the necroptosis machinery are currently known. Early work first demonstrated that necroptosis following tumour necrosis factor receptor 1 (TNFR1) activation is dependent on RIPK1 and RIPK3. This pathway is commonly referred to as canonical necroptosis [4]. Subsequently, it was shown that necroptosis can also occur independently of RIPK1 following activation of Toll/interleukin-1 receptor (TIR) domain-containing adapter-inducing interferon-β (TRIF) or Z-DNA-binding protein 1/DNA-dependent activator of IFN-regulatory factors (ZBP1/DAI) [5–8]. RIPK3 hereby serves as the major component in the

Received: 1 December 2021
Revised: 10 January 2022
Accepted: 11 January 2022

Accepted Manuscript online: 11 January 2022
Version of Record published: 4 February 2022

Biochemical Journal (2022) 479 259–272
https://doi.org/10.1042/BCJ20210677

so-called necrosome, which converges multiple upstream signals to induce necroptosis. Of particular interest here is that RIPK3 is activated via interactions with proteins that contain RIP homotypic interaction motifs (RHIMs) such as RIPK1, TRIF, and ZBP1/DAI [9].

In 2012, it was first demonstrated that association between RIPK1 and RIPK3 via their RHIMs, required for necroptosis, results in the formation of fibrillary structures, termed amyloids [10]. Furthermore, the necrosome, which consists of RIPK3 and MLKL (and in certain settings RIPK1), has an amyloid-like structure [11], and intermolecular RHIM–RHIM interactions are mainly responsible for amyloid formation in necrosomes. RHIMs contain the conserved tetrad core sequence (V/I)-Q-(V/I/L/C)-G, flanked by hydrophobic sequences on both sides. Notably, the structure of the RIPK1–RIPK3–MLKL necrosome has recently been resolved by solid-state NMR. The RIPK1–RIPK3 necrosome is an amyloid-signalling complex that initiates tumour necrosis factor (TNF)α-induced necroptosis. Herein, RIPK1 and RIPK3 alternately stack (RIPK1, RIPK3, RIPK1, RIPK3, etc.) to form heterotypic β-sheets. Two such β-sheets interact along a compact hydrophobic interface featuring an unusual ladder of alternating Ser (from RIPK1) and Cys (from RIPK3) residues [12]. Despite the amyloid characteristics reported to date, it has not yet been possible to fully elucidate which minimal features characterise a functioning RHIM.

Numerous reports by ourselves and others revealed that RIPK1 is a major regulator of signalling pathways that lead to inflammation and RCD, hence RIPK1 has gained considerable interest as a drug target for a spectrum of human diseases [13], including ischemia-reperfusion injury and sepsis [14,15]. Furthermore, studies on RHIM-containing adaptors have unveiled a central role of RIPK1 in controlling several complex pathways related to decisions of cell survival and death [16,17].

RHIM-containing proteins also play a special role in the defence against viral infections. Infection of a cell by various viruses leads to RHIM-mediated cell death, in particular necroptosis [5,18,19]. To ensure their own survival or lifelong infection in the host, specific viruses carry out sophisticated molecular strategies to evade these host cell death responses. For instance, viral proteins like ICP6, encoded by herpes simplex virus 1 (HSV-1), and other members of the Herpesviridae family including the M45 protein from murine cytomegalovirus (MCMV), encode a RHIM domain that inhibits host cell death pathways by forming heteromeric amyloid fibrils with RHIM-containing proteins of the host cell [20]. This indicates that the formation of RHIM-containing amyloid structures is not necessarily accompanied by cell death, and that regulation of cellular life and death following activation of RHIM proteins is far more complicated and context-dependent. Recent atomic force microscopy studies demonstrated that RIPK3 amyloid fibrils can further assemble into large fibrillary networks during necroptosis, and revealed distinct inter-filament interactions in RIPK3 and viral M45 amyloids that contribute to preventing mammalian necroptosis [21]. Formation of viral–host heteromeric amyloid assemblies may underpin a general mechanism of viral adaptation against host immune machineries.

MCMV M45 protein is a RHIM-containing adaptor that, like ZBP1, interacts with cellular RIPK1 and RIPK3 [22], which prompted us to generate a cell-permeable recombinant TAT–M45 fusion protein that should counteract the RHIM–RHIM interactions of RIPK1 and RIPK3 during pathophysiologic cell death processes.

When screening various cancer cell lines and primary cells from different species, we unexpectedly discovered that all tested cells were killed by recombinant TAT–M45 protein in a time- and concentration-dependent manner. Therefore, we changed our primary approach and confirmed this phenomenon by testing a selection of short synthetic TAT–RHIM peptides, ruling out the possibility that the mere presence of the TAT-protein fusion or formation of unfolded protein aggregates induced cell death. Subsequent studies showed that TAT–RHIM has a direct toxic (disruptive) effect on biological membranes. This killing effect is mediated independently of a host cell specific endogenous RHIM domain and cannot be interrupted by any known inhibitor of RCD.

Material and methods

Cloning, expression, and purification of TAT–M45 protein

MCMV DNA (Smith strain) was a kind gift from Dr. Michael Winkler (German Primate Center — Leibniz Institute for Primate Research, Göttingen, Germany). cDNA was generated using the Thermoscript RT-PCR System (Invitrogen, Thermo Fisher Scientific, Schwerte, Germany) with 5′-CAAGGGTACCATGGAT CGCCAGCCCAAAGTC-3′ forward and 5′-CGGGAATTCTTAGTACAGGAGGGGATCAGCTTTAG-3′ reverse primers. The multiple cloning site of the pTAT vector (a kind gift from Prof. Steven F. Dowdy, UCSD School of Medicine, La Jolla, CA, U.S.A.) includes an N-terminal 6-histidine leader, followed by an 11 amino acid TAT protein transduction domain (PTD) and a polylinker [23]. The PCR product was cloned into the *Kpn*I/

*Eco*RI-cut pTAT-vector, and the resulting construct isolated from a colony harbouring the TAT–M45 cDNA was transformed into competent T7 Express *Escherichia coli* BL21(DE3) bacteria (New England BioLabs, Frankfurt, Germany). Expression was induced in Luria Bertani (LB) media with isopropyl-D-thiogalactopyranoside at a final concentration of 0.4 mM. After incubation for 3 h at 37°C, cells were harvested by centrifugation (6 500×***g***, 10 min, 4°C) followed by sonication in binding buffer (300 mM NaCl, 50 mM sodium phosphate, pH 7.0). The lysate was clarified by centrifugation (14 000×***g***, 20 min, 4°C), and supernatant containing TAT–M45 protein was purified under native conditions using pre-equilibrated TALON Metal Affinity Resin (BD Clontech, Heidelberg, Germany). To remove contaminating bacterial proteins, columns were washed by stepwise addition of increasing imidazole concentrations. Finally, target proteins were eluted with elution buffer (300 mM NaCl, 50 mM sodium phosphate, 200 mM imidazole, pH 7.0). Removal of salt was performed using a disposable Sephadex G-25 PD-10 desalting column (Amersham Biosciences, Freiburg, Germany) equilibrated with RPMI medium. An Amicon centrifugal filter (Sigma–Aldrich/Merck Millipore, Taufkirchen, Germany) was used to concentrate the fusion protein, which was used immediately after purification or stored at −20°C. Protein samples were analysed by gel electrophoresis followed by Coomassie Blue staining (Figure 1B).

Synthesis and purification of peptides

Protected peptides (Figures 2A,B, and 3) were synthesised in-house using standard Fmoc/tBu chemistry on a Syro II Multiple Peptide Synthesizer (MultiSyntechTech, Witten, Germany) with acid-labile TCP resin (Intavis, Tübingen, Germany) as described previously [24,25]. After deprotection, peptides were purified by gradient reversed-phase HPLC on a C18 column and their identity was confirmed using electrospray mass spectrometry (ESI-MS) and MALDI-TOF-MS. Peptide purities were ≥95% as determined by analytical reversed-phase HPLC (data not shown). However, large amounts of peptides shown in Figures 2A and 3A,B and I were synthesised commercially by ProteoGenix (Schiltigheim, France) using identical methodology.

Cell lines

RIPK3-expressing NIH3T3-N cells [26], L929, HT-29, and U937 cells were obtained from the American Type Culture Collection (Manassas, VA, U.S.A.). NIH3T3, L929, and HT-29 cell lines were cultured in DMEM (Gibco, Thermo Fisher Scientific) supplemented with 10% (v/v) FCS (PAN-Biotech GmbH, Aidenbach, Germany), 100 U/ml penicillin, and 100 µg/ml streptomycin (both from Merck Millipore GmbH, Darmstadt, Germany). U937 cells were cultured in RPMI 1640 media supplemented with 10% (v/v) FCS, 100 U/ml penicillin, 100 µg/ml streptomycin, 1 mM sodium pyruvate, and 0.25% D-(+)-glucose (Sigma–Aldrich Chemie GmbH, Taufkirchen, Germany). All cell lines were cultured in a humidified 5% CO_2 atmosphere at 37°C. Negativity for mycoplasma was routinely checked using a MycoAlert Mycoplasma Detection Kit (Lonza, Cologne, Germany). Unless stated otherwise, assays were conducted on 1×10^5 cells in 1 ml of medium.

Mice

Nlrp3-knockout (ko) mice (stock no. 021302) were purchased from Charles River (Sulzfeld, Germany). All mice used in this study, including wild-type (wt) animals, were 8-week-old males of the C57BL/6J background. The animals were housed in the Central Animal Facility of the University Hospital Schleswig-Holstein (Kiel, Germany). All mice were maintained on a standard diet and a 12 h day–night rhythm. For isolating bone marrow cells rodents were first anesthetised with isoflurane followed by euthanasia through cervical dislocation. All experiments were performed according to the Protection of Animals Act with the approval of German authorities.

Isolation of bone marrow-derived macrophages (BMDMs)

Bone marrow cells were isolated as described previously [27]. Briefly, segregated cells were differentiated into BMDMs by cultivating in high-glucose RPMI 1640 medium with NEAAs (Gibco, Thermo Fisher Scientific), supplemented with 10% (v/v) FCS, 100 U/ml penicillin, 100 µg/ml streptomycin and 30% (v/v) L929-conditioned medium at 37°C with 5% CO_2 for 6 days. For experiments, cells were plated overnight for stimulation at 4×10^5 cells/ml on 12-well plates in a total volume of 1 ml.

Generating stable CRISPR/Cas9 knockout cell lines

CRISPR/Cas9-edited *Ripk1*-, *Ripk3*-, and *Ripk1/Ripk3/Mlkl* triple deficient NIH3T3 cells were generated as described previously [15,28]. Briefly, sgRNAs for selected targets (TCCCGAAGCCTCCGCTGTCTAGG,

Biochemical Journal (2022) **479** 259–272
https://doi.org/10.1042/BCJ20210677

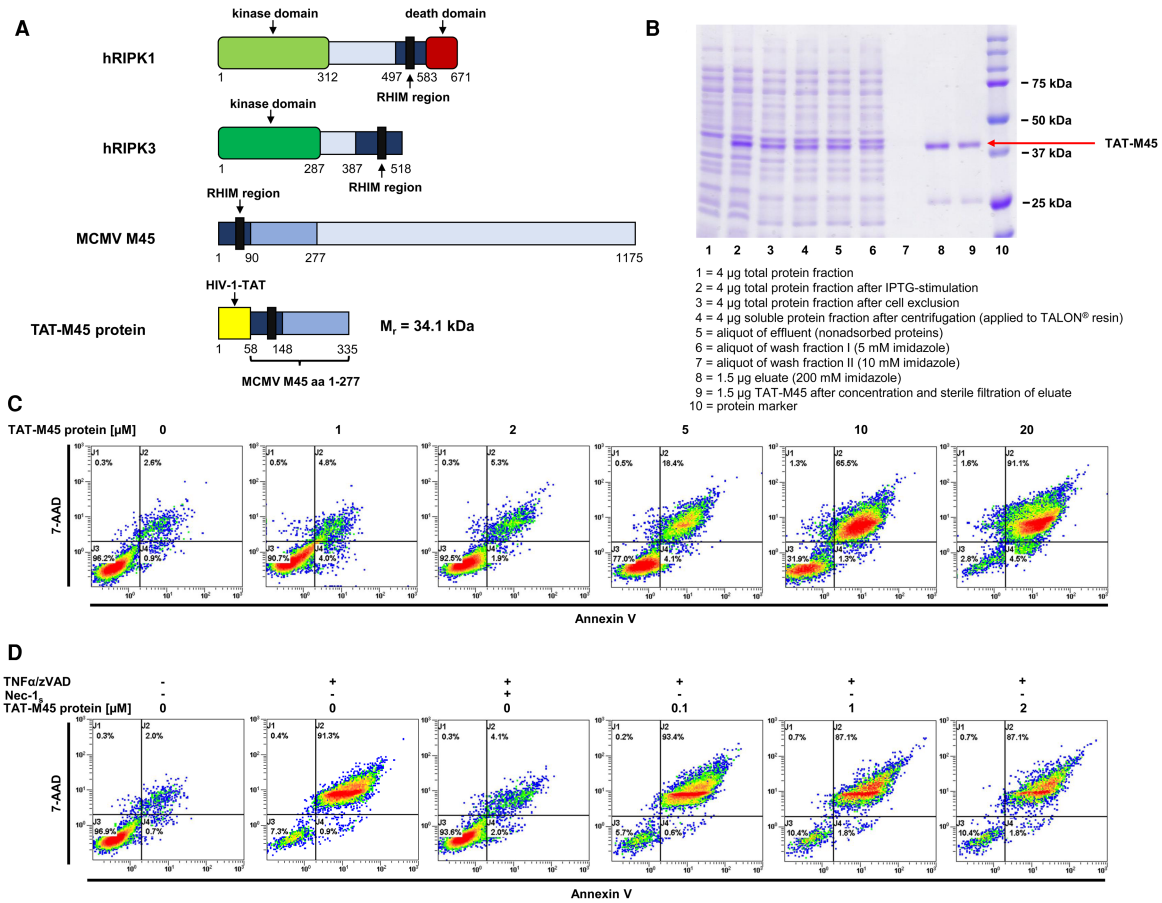

Figure 1. The TAT–M45 protein is cytotoxic by itself and does not inhibit necroptosis.

(**A**) Schematic illustrations of the structure of human receptor-interacting serine/threonine protein kinase (hRIPK) 1 and hRIPK3, the full-length M45 protein of murine cytomegalovirus (MCMV M45) and the TAT–M45 protein that we generated by cloning the coding sequence of the N-terminal region (aa 1–277) of M45 into a TAT vector. (**B**) Fractions of the native soluble polyhistidine-tagged TAT–M45 protein purified using TALON metal affinity resin were analysed via SDS–PAGE. The imidazole-isolated target protein used for our subsequent studies is marked in the Coomassie Blue-stained gel. (**C**) Murine NIH3T3 cells were incubated with the indicated concentrations of TAT–M45 protein for 8 h at 37°C. Cell death was quantified by FACS analysis using 7-amino-actinomycin D (7-AAD) and phosphatidylserine accessibility (Annexin V staining) as markers. FACS dot plots of a representative approach of three independent experiments are shown. Purified TAT–M45 protein induces significant cell death in this setting at concentrations ≥5 µM. (**D**) NIH3T3 cells were incubated with 100 ng/ml TNFα and 25 µM zVAD for 8 h at 37°C to induce necroptosis. RIPK1 inhibitor Nec-1$_s$ (20 µM) or increasing concentrations of TAT–M45 were added as indicated. Cell death was quantified by FACS as described above. A representative of three independent experiments is shown. Note that Nec-1$_s$ inhibits necroptotic cell death in this setting, while TAT–M45 does not.

AACCCGAGTGCCCTCGGCCCTGG and GCACACGGTTTCCTAGACGCTGG for *Ripk1*, *Ripk3*, and *Mlkl*, respectively, and all three for generating the *Ripk1/Ripk3/Mlkl* triple knockout were designed *in silico* using the CRISPR Design Tool (http://chopchop.cbu.uib.no/). Single-stranded sgRNA oligos were annealed and ligated into an expression plasmid bearing both the sgRNA scaffold backbone and Cas9 (pX330-U6-Chimeric_BB-CBh-hSpCas9, Addgene Plasmid no. 42230). The resulting plasmid (pSpCas9_sgRNA) was then co-transfected with the pcDNA3.1(+) vector (Invitrogen, Thermo Fisher Scientific, no. V790-20) containing a geneticin resistance gene into target cells. After single-cell cloning by serial dilution in 96-well plates (media was supplemented with 1 mg/ml G418), clones were assayed and selected for their target gene-knockout by western blotting analysis to identify stable CRISPR/Cas9-ko cell lines (data not shown). To exclude feasible off-target effects or clonal variations within the cell population we generated and analysed three different guide RNAs for each target gene(s) and observed congruent outcomes in each case (data not shown).

Biochemical Journal (2022) **479** 259–272
https://doi.org/10.1042/BCJ20210677

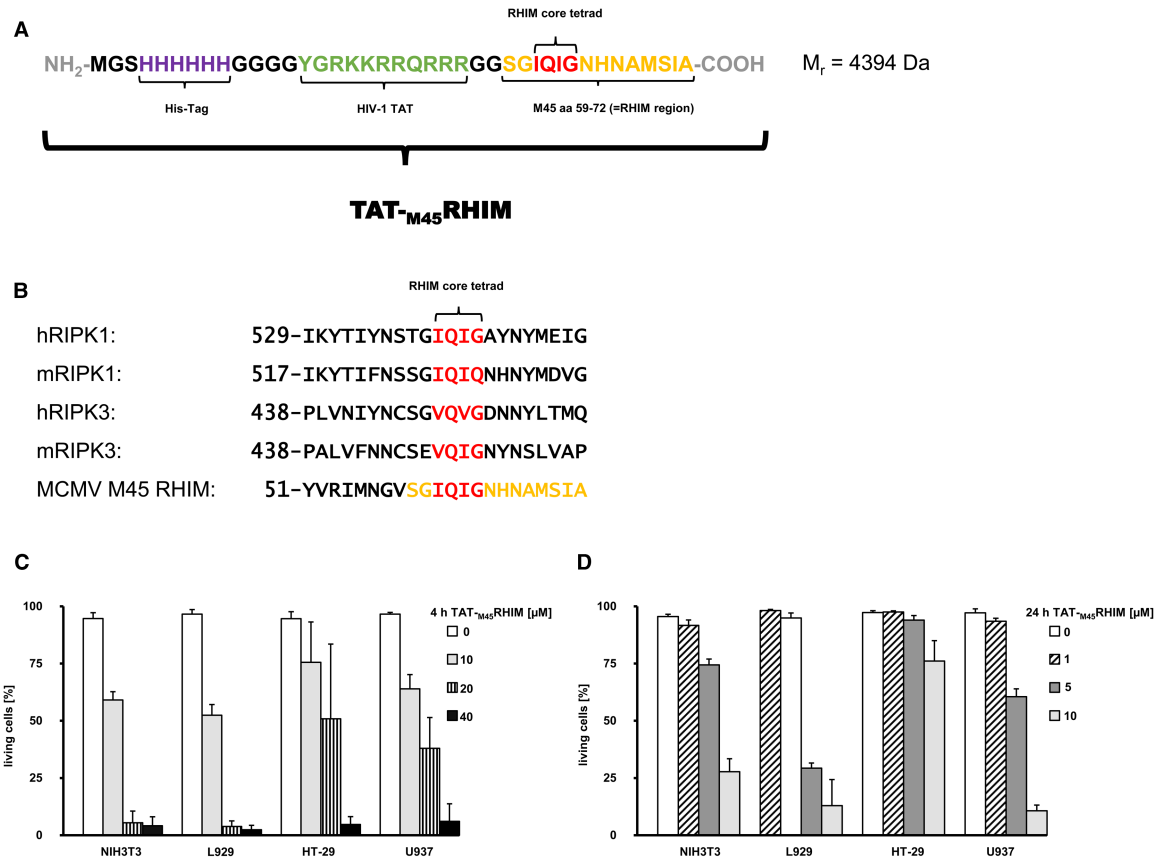

Figure 2. Structure and properties of the TAT–$_{M45}$RHIM peptide.

(**A**) Illustration of the amino acid sequence of the TAT–$_{M45}$RHIM peptide. The peptide consists of an N-terminal polyhistidine tag (purple), 11 crucial amino acids of the HIV-1 TAT protein (green) and 14 amino acids of the M45-RHIM region (yellow) which contains the conserved RIP homotypic interaction motif (RHIM) core tetrad (red). (**B**) Amino acid sequences of the RHIM regions of human and mouse receptor-interacting serine/threonine protein kinase 1 and 3 (h/mRIPK1/3) and MCMV M45. Note the cross-species conserved RHIM core tetrad (red) and the M45 sequence used for TAT–$_{M45}$RHIM (yellow). (**C**) Murine NIH3T3 and L929 fibroblasts as well as human HT-29 and U937 cells were incubated with the indicated concentrations of TAT–$_{M45}$RHIM for 4 h. The percentage of surviving cells was then determined by FACS analysis using 7-AAD and phosphatidylserine accessibility (Annexin V staining) as cell death markers. The graphs present the means ± standard deviations of three independent experiments. (**D**) Murine NIH3T3 and L929 fibroblasts as well as human HT-29 and U937 cells were incubated with the indicated (reduced) concentrations of TAT–$_{M45}$RHIM for 24 h. The percentage of surviving cells was then determined by FACS analysis using 7-AAD and phosphatidylserine accessibility (Annexin V staining) as cell death markers. The graphs present the means ± standard deviations of three independent experiments.

Reagents

Restriction enzymes *Kpn*I (R0142) and *Eco*RI (R0101) were obtained from New England BioLabs. Recombinant purified TNFα (570104) was purchased from BioLegend (Amsterdam, Netherlands). The pan-caspase inhibitor zVAD-fmk (4026865) was purchased from Bachem (Weil am Rhein, Germany) and Nec-1$_s$ (2263-1-BV) was obtained from BioCat (Heidelberg, Germany). Isopropyl-D-thiogalactopyranoside (I6758) and primidone (P7295) were purchased from Sigma–Aldrich/Merck Millipore. Etanercept was obtained from Pfizer Pharma GmbH (Berlin, Germany). For fluorescence microscopy, we used anti-Penta-His antibody (34660, Qiagen, Hilden Germany) and TRITC-Donkey IgG anti-Mouse IgG (H + L) (715-025-150, Dianova, Hamburg, Germany). Slides were mounted using ImmunoSelect Antifading Mounting Medium with DAPI (SCR-038448, Dianova).

Biochemical Journal (2022) **479** 259–272
https://doi.org/10.1042/BCJ20210677

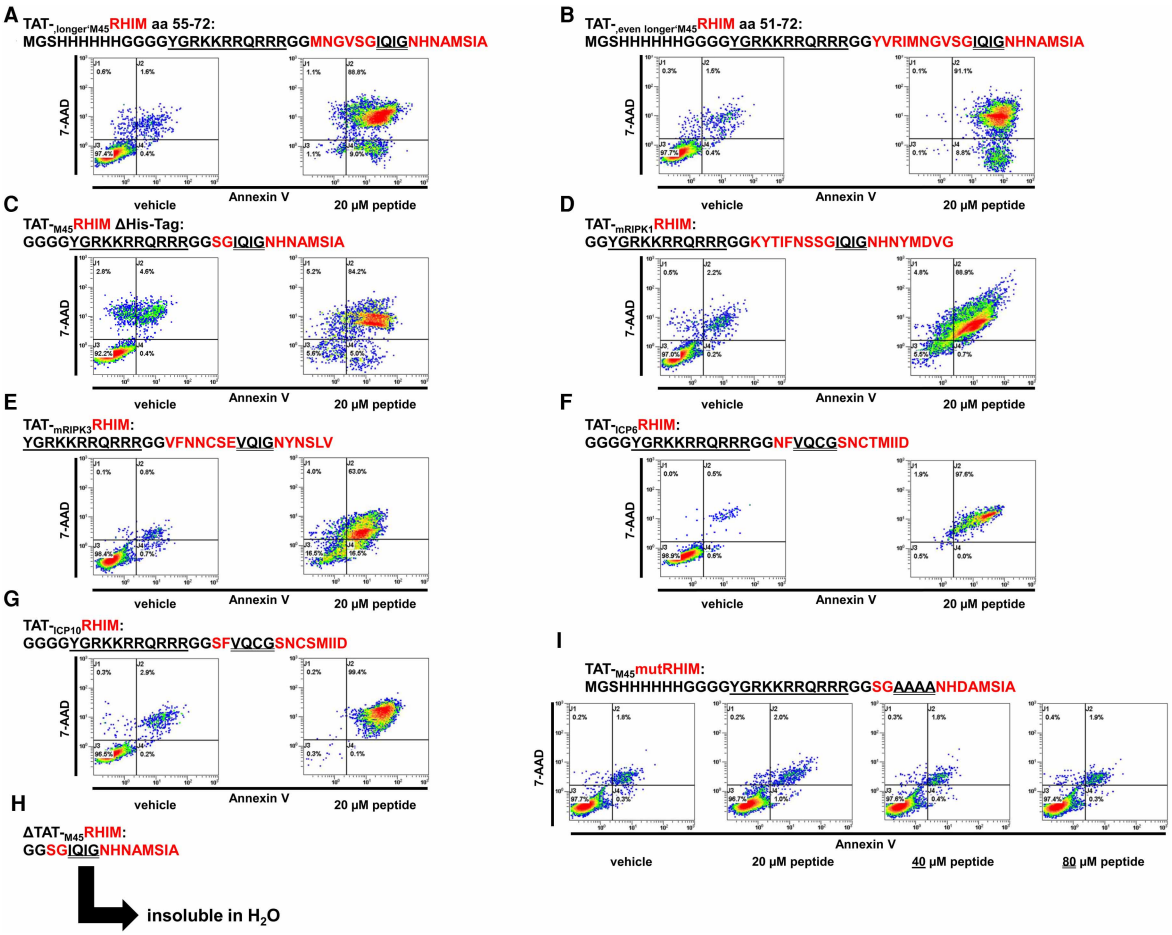

Figure 3. TAT–RHIM peptides are universally cytotoxic, except for the TAT–$_{M45}$mutRHIM variant.

In all panels, the amino acid sequence of the respective TAT–RHIM variant under investigation is shown at the top. The TAT sequence is underlined in each case, the RHIM sequence is shown in red and the conserved RHIM core tetrad therein is black and double underlined. Below, representative dot plots of NIH3T3 cells incubated with or without the abovementioned TAT–RHIM variant at the indicated concentrations for 24 h at 37°C are shown. Cell death was quantified by FACS analysis using 7-AAD and phosphatidylserine accessibility (Annexin V staining) as markers. (**A**) The TAT–$_{,longer'M45}$RHIM variant shown here includes four additional N-terminal amino acids (MNGV) of the M45-RHIM region. (**B**) The TAT–$_{,even\ longer'M45}$RHIM variant shown here includes eight additional N-terminal amino acids (YVRIMNGV) of the M45-RHIM region. (**C**) TAT–$_{M45}$RHIM ΔHis-Tag lacking the N-terminal polyhistidine tag of the 'original' TAT–$_{M45}$RHIM peptide. (**D**) TAT–$_{mRIPK1}$RHIM with the RHIM region sequence of murine RIPK1 and only two glycines on the N-terminal end. (**E**) TAT–$_{mRIPK3}$RHIM has the RHIM region sequence of murine RIPK3 and no glycine on the N-terminal end, directly starting with the TAT sequence. (**F**) TAT–$_{ICP6}$RHIM containing the RHIM sequence of the ICP6 protein from HSV-1 but no polyhistidine tag. (**G**) TAT–$_{ICP10}$RHIM containing the RHIM sequence of the ICP10 protein from HSV-2 but no polyhistidine tag. (**H**) The ΔTAT–$_{M45}$RHIM variant consisting only of the M45-RHIM sequence, which is insoluble in water and could, therefore, not be used for experiments in cell culture. (**I**) In the TAT–$_{M45}$mutRHIM variant, the four conserved amino acids IQIG of the M45-RHIM core tetrad are replaced by AAAA. In contrast with all other TAT–RHIM variants studied, this variant showed no cytotoxicity even at concentrations up to 80 μM for 24 h. FACS dot plots of a representative approach from each of three independent experiments are shown.

Flow cytometry analysis of cell death

Phosphatidylserine exposure to the outer cell membrane of apoptotic cells or inner plasma membrane of necrotic cells and incorporation of 7-amino-actinomycin D (7-AAD) into necrotic cells was quantified by flow cytometry analysis. After stimulation of cells under the indicated conditions, staining was performed on single-cell suspensions using FITC Annexin V (BioLegend, 640906) and 7-AAD Viability Staining Solution

(BioLegend, 420404) according to the manufacturer's instructions. Fluorescence was analysed using an FC-500 flow cytometer (Beckman Coulter GmbH, Krefeld, Germany).

Fluorescence microscopy

L929 cells were seeded overnight on 8-well chamber slides at 2×10^4 cells in 200 µl DMEM supplemented with 10% (v/v) FCS, 100 U/ml penicillin, and 100 µg/ml streptomycin. Following incubation with 40 µM TAT–$_{M45}$RHIM, cells were fixed in 4.5% formalin, blocked with horse serum, permeabilised with Triton X-100, and stained for the His-Tag of TAT–$_{M45}$RHIM using an anti-Penta-His antibody and TRITC-Donkey IgG anti-Mouse IgG (H + L). Slides were mounted using ImmunoSelect Antifading Mounting Medium with DAPI. Imaging was performed using a Zeiss Axio Imager Z1 fluorescence microscope and AxioVision Rel. 4.8 software (Carl Zeiss GmbH, Jena, Germany). Figures were prepared using Fiji/ImageJ software. Greyscale images were assigned the respective pseudocolour, and channels were merged. Gamma correction (gamma-value = 0.9) was uniformly applied to prepare images for publication.

Pyranine efflux assay

Lipid films (2 mg) composed of 1-palmitoyl-2-oleoyl-*sn*-glycero-3-phosphocholine (POPC) were prepared from chloroform stock solution. Chloroform was evaporated under an N_2-stream and the lipid film was dried for 3 h *in vacuo* at room temperature. The lipid film was incubated with 100 mM pyranine in 500 µl buffer (100 mM KCl, 20 mM HEPES, pH 7.4) for 30 min. The mixture was vortexed three times for 30 s in 5 min intervals and then extruded through a polycarbonate membrane (diameter 200 nm, LiposoFast-Basic, Avestin, Ottawa, IL, U.S.A.). The external buffer was exchanged against 275 mM KCl, 20 mM HEPES, pH 7.4, by gel filtration using a Sephadex G-25M prepacked PD-10 column (Global Life Science Solutions Operations U.K. Ltd., Buckinghamshire, U.K.). The lipid concentration was determined via a phosphate test as described previously [29]. The vesicle suspension was diluted to 800 µl (c_{lipid} = 50 µM). Pyranine efflux and dequenching were monitored using a fluorescence spectrometer (T = 20°C, λ_{ex} = 460 ± 5 nm, λ_{em} = 512 ± 5 nm, data pitch = 0.2 s, sensitivity = 350 V; FP-6500, Jasco GmbH, Gotha, Germany). TAT–$_{M45}$RHIM (c_{stock} = 1 mM in H_2O; c_{final} = 0.5–10 µM) was added at t = 0 s. After t > 200 s the vesicles were lysed using 10 µl 10% (w/v) Triton X-100. The intensity was normalised (I_{norm}) to the values before (t = − 25 s) addition of TAT–$_{M45}$RHIM (I_0) and after lysis (I_{end}) using the following formula:

$$I_{norm} = \frac{I_t - I_0}{I_{end} - I_0}$$

Results

Necroptosis plays a critical role in many clinically relevant human diseases, hence its inhibition may offer promising therapeutic approach in many settings [30]. Blockade of host-specific necroptosis in infected cells by various RHIM orthologs is a conserved and highly effective mechanism employed by several herpesviruses [31]. The potential therapeutic use of a viral RHIM ortholog is, therefore, obvious. Initially, we believed that the M45 protein of MCMV was particularly promising in this regard because, in contrast with HSV-RHIM proteins, for example, it inhibits necroptosis equally in both human and murine systems [32]. However, to make M45 therapeutically useful via external delivery, a vehicle is needed to transport the protein into cells. Analyses of the native M45 protein, consisting of 1175 amino acids (aa), demonstrated that the N-terminal region of the protein, also containing the required RHIM domain, is sufficient for M45-mediated cell death suppression [16]. Thus, in order to increase the solubility of the recombinant protein, we cloned only the coding sequence of the N-terminal region (aa 1–277) of the viral protein into the TAT vector [33]. We first synthesised a recombinant TAT–M45 fusion protein consisting of 58 aa, including the truncated TAT domain of HIV-1 (11 aa) and aa 1–277 of M45 (Figure 1A). TAT–M45 was readily soluble and appeared slightly larger than 37 kDa on Coomassie Blue-stained gel (Figure 1B). Unexpectedly, starting at a concentration of 5 µM in all cell lines studied, the protein displayed pronounced cytotoxicity (Figure 1C), unlike any of the TAT fusion proteins we had synthesised and tested before [33,34]. Unfortunately, however, we failed to detect any inhibitory effect on necroptosis even at lower concentrations (Figure 1D).

Since we were initially unable to elucidate the reasons for the pronounced cytotoxicity observed for the TAT–M45 protein, we decided to generate a peptide that was as small as possible and contained only the TAT

Biochemical Journal (2022) **479** 259–272
https://doi.org/10.1042/BCJ20210677

and M45 residues (Figure 2A). This TAT–$_{M45}$RHIM peptide (M_r = 4394 Da) enclosed only the N-terminal poly-histidine tag for detection via α-His-Tag antibody, the 11 aa of the TAT protein that are crucial for translocation across the plasma membrane [35], flanked by glycine spacers, and 14 aa of the M45-RHIM region, containing the conserved 4 aa RHIM core tetrad indispensable for interaction with other RHIM-containing proteins (Figure 2B). This peptide was again readily soluble, but, surprisingly, just like the TAT–M45 protein, it exhibited a time- and concentration-dependent cytotoxic effect at a concentration of ∼5 μM in all cell lines tested (Figure 2C,D). However, like the larger TAT–M45 protein, TAT–$_{M45}$RHIM peptide showed no inhibitory effect on necroptosis in human or murine cells at lower concentrations (data not shown).

Since we had never observed such cytotoxicity before for TAT proteins, we assumed that the specific M45-RHIM sequence might be responsible. We, therefore, synthesised TAT–RHIM peptides with a wide variety of different RHIM sequences. Valine (aa 58) in M45 located three positions upstream of the conserved RHIM core tetrad IQIG may be crucially involved in the interaction between RIPK3 and M45, and thus essential for the inhibitory properties of M45 in necroptosis [36]. If true, our original TAT–$_{M45}$RHIM peptide would have been too short, because the RHIM sequence we initially chose from M45 did not start until one amino acid after this valine. We, therefore, generated two TAT–RHIM variants including this valine. Unfortunately, neither differed from our original peptide (Figure 3A,B). Next, we generated an even shorter TAT–RHIM peptide without the His-Tag (denoted ΔHis-Tag). Yet again, this peptide was cytotoxic (Figure 3C) and also failed to inhibit necroptosis (data not shown). We then tried TAT–RHIM constructs with the RHIM sequences of murine RIPK1 and RIPK3 truncated and leaving out the initial spacer glycines that originally linked the His-Tag to the TAT peptide. Even with these, we could only detect cell death, but no inhibition of regulated necrosis (Figure 3D,E). ICP6 and ICP10 proteins from HSV-1 and HSV-2 are viral RHIM orthologs known to inhibit necroptosis via RHIM–RHIM interactions [32]. We originally refrained from using these RHIM sequences, since ICP6 and ICP10 prevent necroptosis only in human cells, whereas they do exactly the opposite in murine cells, which would complicate studies *in vitro* and would prevent their use in animal models [37]. However, given our previous findings, we wanted to investigate whether using these sequences would yield different results. As expected, the respective TAT–RHIM peptides killed murine cells like the previous ones (Figure 3F,G), but unexpectedly they also killed human cells and had no inhibitory properties on necroptosis in these cell lines (data not shown). Next, to investigate whether the combination of the TAT peptide and the RHIM domain was responsible for the cytotoxic effect, we synthesised a RHIM peptide containing only the M45-RHIM domain without the TAT moiety (Figure 3H). With a calculated molecular mass of only 1527 Da, we predicted that this peptide could be a freely diffusing biomolecule that would easily cross the cell membrane, but unfortunately, it was insoluble in water.

The inhibitory effect of M45 on necroptosis is dependent on its RHIM core tetrad IQIG. If this sequence is substituted to AAAA, M45 loses its protective effect [16]. Therefore, to investigate whether the cytotoxic effect of our peptide is also dependent on the RHIM core tetrad, we synthesised the AAAA (mutRHIM) variant of the TAT–$_{M45}$RHIM peptide. To our surprise, this peptide showed no cytotoxicity whatsoever *in vitro* even at concentrations up to 80 μM (Figure 3I). Based on this phenomenon, we assumed that the cytotoxicity of our peptides must be a form of RCD that involves known RHIM proteins and the necroptosis machinery.

Strikingly, the pan-caspase inhibitor zVAD-fmk, the RIPK1 inhibitors Nec-1$_s$ and primidone, and the TNF antagonist etanercept [14,15] could not inhibit TAT–$_{M45}$RHIM-induced necrosis (Figure 4A). We then investigated whether knockout of the endogenous RHIM proteins and necroptosis effectors RIPK1 and RIPK3 alone or in combination with the terminal necroptosis effector MLKL would provide any resistance against TAT–$_{M45}$RHIM-induced cell death. Although the *Ripk1*, and *Ripk3* single knockout and also the *Ripk1/Ripk3/Mlkl* triple knockout cell lines were maximally protected against TNFα-induced necroptosis, they resembled non-edited (parental) cells in terms of their reaction with TAT–$_{M45}$RHIM (Figure 4B). By comparing primary BMDMs isolated from C57BL/6 wt mice and *Nlrp3*-ko mice, respectively, we could also rule out any role of canonical pyroptosis [38] in TAT–$_{M45}$RHIM-induced cell death (Figure 4C).

On this basis, we assumed that TAT–$_{M45}$RHIM-induced necrosis is not a regulated process. We now believed that the peptide, with its combination of polycationic TAT moiety and hydrophobic RHIM domain predisposed to self-oligomerisation, could have a direct destructive effect on biomembranes. Similar effects have been previously described for other arginine-rich peptides [39]. By applying fluorescence microscopy, we observed that our added TAT–$_{M45}$RHIM peptide accumulates in cells after a short incubation period, and massive changes in the cell membrane and subsequent necrosis occur within 2 h (Figure 5A,B). Direct permeabilisation of phospholipid membranes by TAT–$_{M45}$RHIM was also reproducible in a biomimetic system; after addition of

Biochemical Journal (2022) **479** 259–272
https://doi.org/10.1042/BCJ20210677

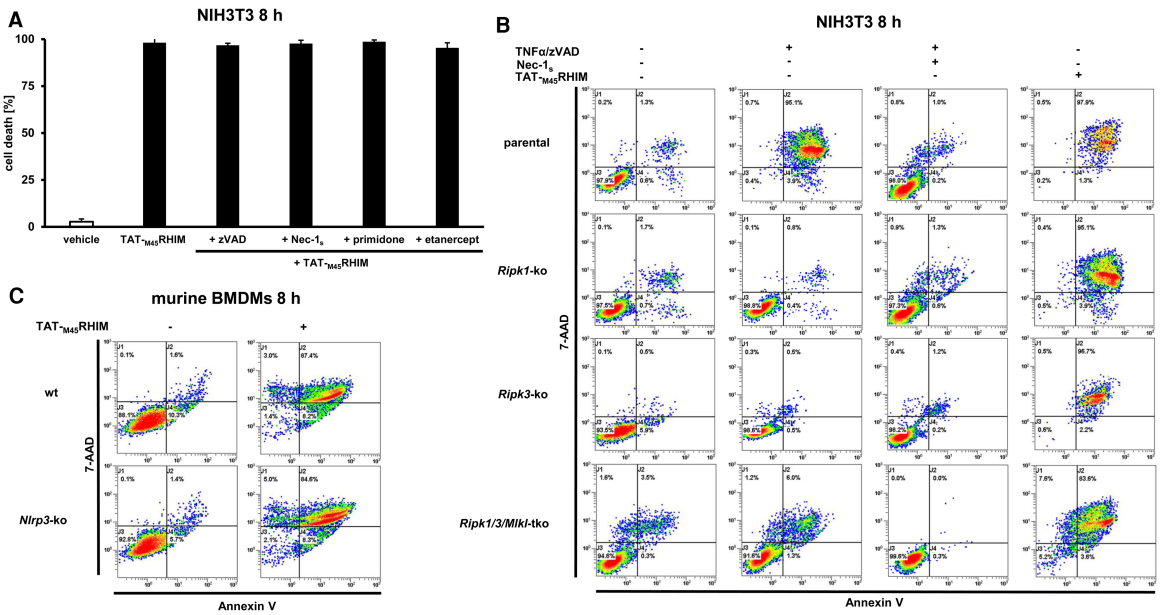

Figure 4. TAT–RHIM induces necrotic cell death that is independent of endogenous RHIM proteins and cannot be inhibited.

(**A**) Murine NIH3T3 cells were incubated with 40 μM TAT–$_{M45}$RHIM for 8 h in the presence of either 25 μM of the pan-caspase inhibitor zVAD, 20 μM of the RIPK1 inhibitor Nec-1$_s$, 1 mM of the RIPK1 inhibitor primidone, or 10 μg/ml of the TNF antagonist etanercept. Cell death was quantified by FACS analysis using 7-AAD and phosphatidylserine accessibility (Annexin V staining) as markers. The graphs present the means ± standard deviations of three independent experiments. None of the investigated inhibitors of RCD could ameliorate TAT–$_{M45}$RHIM-induced cell death. (**B**) Murine non-edited, *Ripk1*-, *Ripk3*- or *Ripk1*/*Ripk3*/*Mlkl*-edited NIH3T3 cells (designated as parental, *Ripk1*-ko, *Ripk3*-ko and *Ripk1/3/Mlkl*-tko, respectively) were incubated for 8 h at 37°C as indicated with 100 ng/ml TNFα + 25 μM zVAD, 20 μM Nec-1$_s$, or 40 μM TAT–$_{M45}$RHIM. Cell death was quantified by FACS analysis using 7-AAD and phosphatidylserine accessibility (Annexin V staining) as markers. FACS dot plots of a representative experiment are shown ($n = 3$ independent repeats). While TNFα/zVAD induces necroptosis in parental NIH3T3 cells that can be rescued by Nec-1$_s$, the respective *Ripk1*, *Ripk3* single- or *Ripk1/3/Mlkl* triple knockout cells are completely protected against necroptosis. Nevertheless, like non-edited cells, these ko-cells are as susceptible to TAT–$_{M45}$RHIM-induced cell death. (**C**) Primary murine BMDMs isolated from wild-type (wt) or *Nlrp3*-knockout (*Nlrp3*-ko) mice were incubated at 37°C with 40 μM TAT–$_{M45}$RHIM for 8 h as indicated. Cell death was quantified by FACS analysis using 7-AAD and phosphatidylserine accessibility (Annexin V staining) as markers. FACS dot plots of a representative experiment are shown ($n = 3$ independent repeats). Note that knockout of *Nlrp3* has no protective effect against TAT–$_{M45}$RHIM-induced cell death.

TAT–$_{M45}$RHIM a rapid permeabilisation of large unilammellar vesicles (LUVs) was detectable at concentrations ≥5 μM (Figure 5C). This corresponds to the concentration at which the cytotoxic effect of the peptide starts in cell culture.

In summary, our results indicate that recombinant proteins and peptides consisting of TAT and any form of RHIM sequence universally induce necrosis, unless the RHIM core tetrad is removed. This process is neither dependent on the known necroptosis machinery nor the NLRP3 inflammasome and we were not able to inhibit it by any means. The resulting loss of membrane integrity is instead caused by direct permeabilisation by TAT–RHIM derivatives.

Discussion

Our initial goal was to establish a new approach for the therapeutic inhibition of necroptosis in human diseases. We drew inspiration for this from naturally occurring viruses; inflammatory cell death in viral infections usually leads to elimination of the virus from the host. To prevent this, some viruses have evolved sophisticated mechanisms, especially members of the Herpesviridae family. Cytomegaloviruses as well as HSV-1 and HSV-2 are known to encode multiple death inhibitors that are required for efficient viral replication and to prevent

Biochemical Journal (2022) **479** 259–272
https://doi.org/10.1042/BCJ20210677

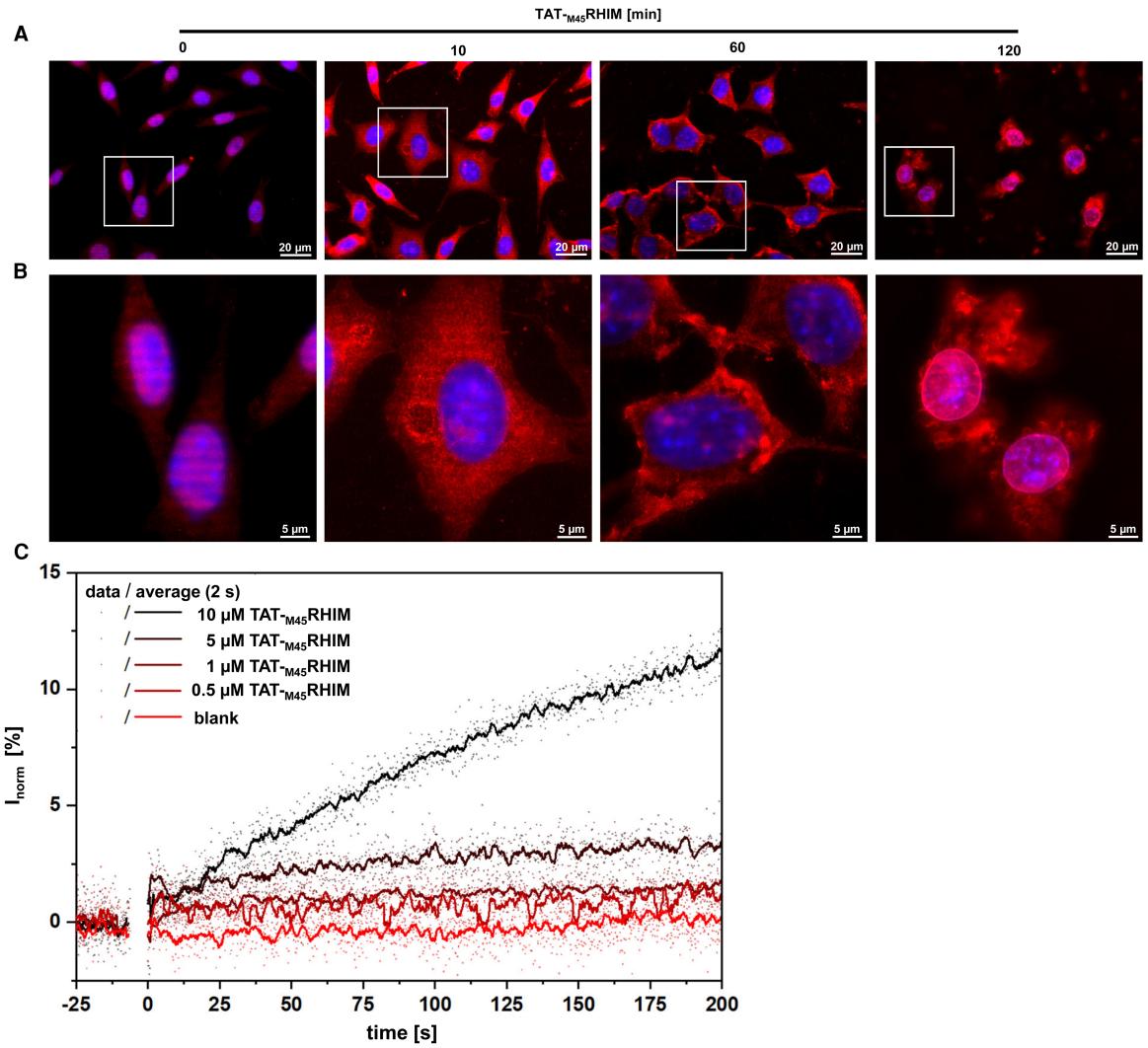

Figure 5. TAT–$_{M45}$RHIM-induced necrosis involves direct disruption of biomembranes.

(**A**) Overlay images of fluorescence microscopy analysis of murine L929 cells incubated with 40 µM TAT–$_{M45}$RHIM for the indicated durations. Samples were stained for the polyhistidine tag of TAT–$_{M45}$RHIM (red), and DAPI (blue) was used for nuclear counterstaining. (**B**) Enlarged images of the labelled sections in (**A**). It is apparent that the peptide initially distributes evenly, and subsequently accumulates in destroyed sections of the cell membrane. (**C**) Time-dependent change in normalised fluorescence intensity (I_{norm}). TAT–$_{M45}$RHIM was added ($t = 0$ s) to POPC-LUVs (50 µM) in 275 mM KCl, 20 mM HEPES, pH 7.4, encapsulating the fluorophore pyranine (100 mM). Due to dye efflux, an increased fluorescence intensity is observed for TAT–$_{M45}$RHIM at concentrations ≥5 µM. After 200 s, I_{norm} increased by ∼3% (5 µM) and ∼12% (10 µM), respectively. Lower TAT–$_{M45}$RHIM concentrations and the blank control show no pyranine efflux upon addition. I_{norm} calculation was performed as described in the 'Material and methods'.

death of the host cell [40]. In practice, these viruses encode a viral inhibitor of caspase activation (vICA) to prevent death receptor (DR)-mediated apoptosis, but this may sensitise the cells to necroptosis. To escape this fate, the virus also encodes a viral inhibitor of RIP activation (vIRA) which disrupts the RHIM-dependent RIPK1–RIPK3 interaction that is critical for TNFα-induced necroptosis, as well as a RIPK3–RHIM-dependent step in virus-induced necrosis [41].

To this end, we aimed to generate a recombinant fusion protein that could penetrate cells efficiently and, analogous to viral RHIM proteins, inhibit necroptosis by preventing the critical RHIM–RHIM interactions during formation of the necrosome. Using the PTD TAT from HIV-1 as a vehicle, we successfully generated a variety of

fusion proteins in the past that were cell-permeable and biologically active [33,34]. We predicted that MCMV M45 would be a promising viral RHIM candidate, because M45 is naturally produced during infection as a full-length protein that is cleaved after residue 277, and this truncated stretch (aa 1–277) is sufficient to inhibit necroptosis in both human and murine cells [32]. Although there is no restriction on the size or type of the delivered cargo, the capacity for successful uptake of cargoes into cells increases when the cationic PTD is attached to lower molecular mass compounds [23]. As shown in Figure 1B, we were able to purify a recombinantly expressed TAT–M45 fusion protein under native conditions, but the protein did not show the desired effect of inhibiting necroptosis (Figure 1D). On the contrary, it was instead cytotoxic at concentrations ≥5 μM (Figure 1C). Therefore, we changed our primary approach and generated a short synthetic TAT–RHIM peptide (TAT–$_{M45}$RHIM, Figure 2A), ruling out that the mere presence of the TAT protein or formation of unfolded protein aggregates induced the observed cell death. By screening a plethora of cancer cell lines and primary cells of different species, we surprisingly discovered that all tested cells were also directly killed by the TAT–$_{M45}$RHIM peptide in a time- and concentration-dependent manner (Figure 2C,D). The rapid onset of cell death suggests that no transcriptional processes are involved in the regulation of TAT–$_{M45}$RHIM sensitivity (at even higher concentrations of the peptide, most cells die within 2 h; data not shown).

RHIM-containing proteins most likely appeared early in the evolution of complex life and, while conserved among mammals, RHIM-like motifs are found in fungi and Drosophila [42,43]. In mammals including humans and mice there are exactly four RHIM-containing proteins and these are the previously mentioned RIPK1, RIPK3, DAI/ZBP1, and TRIF. In general, for RHIM–RHIM interactions, especially the RHIM core tetrad is of great importance. This feature, which as the name suggests consists of 4 aa residues, is highly conserved across mammals and their viruses [44]. We, therefore, speculate that maybe the mere presence of a RHIM motif could be responsible for the observed toxic effect of the TAT–RHIM protein/peptide. However, for the cytotoxic effect of TAT–RHIM, the origin of the RHIM sequence does not seem to play a role, since we tested almost all known viral RHIM sequences as well as 'native' RHIM from murine RIPK1 and murine RIPK3, and always observed the same toxic effect (Figure 3), with no inhibition of TNFα-induced necroptosis in any of the tested cell lines (data not shown). The only known viral RHIM sequence that we did not examine is that from varicella zoster virus (VZV). VZV also encodes a viral RHIM protein, namely open reading frame (ORF) 20. However, we decided not to generate a TAT–$_{ORF20}$RHIM because ORF20 is only thought to bind DAI/ZBP1 and thus prevent DAI/ZBP1-induced apoptosis in the course of VZV infection [45]. For necroptosis in general, and especially for TNFα-induced necroptosis, ORF20 should have no effect, in contrast with the other viral RHIM proteins we tested. Furthermore, human CMV (HCMV) can also block necroptosis, but not through a viral RHIM protein; rather, it acts in a way that is still not completely understood, downstream of activated (phosphorylated) MLKL [18], hence we could not generate a TAT–RHIM based on HCMV.

To exclude the possibility that the combination of the TAT and RHIM alone was responsible for the cytotoxic effect, we synthesised a RHIM peptide that encompassed only the short RHIM domain of M45 without the TAT moiety (Figure 3H), which we assumed should be taken up by cells by passive diffusion. Regrettably, this peptide was completely insoluble in water, preventing this experiment. Although the cytotoxicity of TAT–RHIM does not, according to our experiments performed so far, depend on the origin of the RHIM sequence, we nevertheless demonstrated that the RHIM core tetrad is indispensable for this effect. The mutated RHIM variant of the TAT–$_{M45}$RHIM peptide, in which the four critical amino acids of the RHIM core tetrad were replaced by AAAA, was not at all cytotoxic, even at much higher concentrations than all other TAT–RHIM variants tested (Figure 3I). Thus, it is clear that there is much left to learn about these viruses.

From the results shown in Figure 3I, we hypothesised that the cytotoxicity of all the other TAT–RHIM peptides tested previously might be a form of RCD based on interactions with endogenously expressed RHIM proteins and the necroptosis machinery. Again, we falsified this hypothesis, because neither common pharmacological inhibitors of necroptosis or other RCD processes, nor knockout of endogenously expressed RHIM proteins, had any protective effect on TAT–$_{M45}$RHIM-induced cell death (Figure 4A,B).

Next, we speculated that transduced RHIM peptides in increasing concentrations (i.e. supersaturation) may form intermolecular amyloid aggregates through self-assembly. If so, these homo-oligomers could associate with cellular membranes, directly or indirectly altering plasma membrane integrity, and inducing amyloid-induced lysis, as described previously [46]. This hypothesis would also be consistent with the discovery that functional RHIM amyloids in mammals are composed of hetero-oligomeric fibrils containing mixtures of dissimilar RHIM proteins. However, pathologically accumulated amyloids are predominantly constituted from homo-oligomeric fibrils [47,48]. Involvement of the NLRP3 inflammasome in this process, which is potentially

Biochemical Journal (2022) **479** 259–272
https://doi.org/10.1042/BCJ20210677

activated by amyloids [49], was ruled out by our results showing in Figure 4C. In contrast, we demonstrated that TAT–$_{M45}$RHIM rapidly leads to loss of cell membrane integrity. In an *in vitro* set-up with LUVs, this disruptive effect on biomembranes was found to be independent of any types of (RHIM-containing) cellular proteins and pathways, but TAT–$_{M45}$RHIM could directly permeabilise biomembranes (Figure 5C).

In summary, our plan to design a specific, therapeutically applicable inhibitor of necroptosis failed unexpectedly. Instead, we created a substance that can efficiently destroy all cells that encounter it. Even the sturdiest tumour cell lines of various origins, including murine lymphoblast J558, human osteosarcoma U-2 OS, and human glioma U-87 MG, which have the greatest possible intrinsic resistance to RCD, were killed by TAT–$_{M45}$RHIM and its derivatives (data not shown) in a manner distinct from known forms of (regulated) necrosis. However, this discovery could lead to a new field of application for these peptides. Induction of immunogenic necrotic cell death in malignant tumours represents a potentially important development for oncologic therapies [50]. Resistance of tumour cells to different forms of RCD often results in tumour cells that are refractory to chemotherapeutic agents [51]. Remarkably, TAT$_{M45}$–RHIM-induced necrosis in all tested cell lines. Thus, it would conceivable that it could do so in malignant tumours, and our peptides are available for such studies.

Data Availability

All data and reagents are available from the authors upon request.

Competing Interests

The authors declare that there are no competing interests associated with the manuscript.

Funding

This work was supported by Dr. Werner Jackstädt-Stiftung, Fresenius Medical Care, Germany and Else Kröner-Fresenius Stiftung (to S.K.). This work was additionally funded by the Medical Faculty of CAU Kiel, Germany (to B.K. and S.K.).

CRediT Author Contribution

Stefan Krautwald: Conceptualization, resources, data curation, formal analysis, supervision, funding acquisition, validation, investigation, visualization, methodology, writing—original draft, project administration, writing—review and editing. **Benedikt Kolbrink**: Formal analysis, investigation, visualization, writing—original draft, writing—review and editing. **Theresa Riebeling**: Data curation, formal analysis, validation, investigation, visualization, methodology. **Nikolas K. Teiwes**: Formal analysis, investigation, visualization, methodology. **Claudia Steinem**: Formal analysis, validation. **Hubert Kalbacher**: Data curation, validation, investigation, methodology. **Ulrich Kunzendorf**: Supervision, validation.

Acknowledgements

We thank Maike Noetzel, Katja Bruch and Neele May Garling for excellent technical assistance. Furthermore, we thank the former lab members Federica De Zen, Christine Dewitz, and Caroline Moerke for their excellent help at the initial phase of the study.

Abbreviations

7-AAD, 7-amino-actinomycin D; BMDMs, bone marrow-derived macrophages; DR, death receptor; HCMV, human CMV; HIV-1, human immunodeficiency virus 1; HSV-1, herpes simplex virus 1; LUVs, large unilammellar vesicles; MCMV, murine cytomegalovirus; MLKL, mixed lineage kinase domain-like protein; ORF, open reading frame; PTD, protein transduction domain; RCD, regulated cell death; RHIM, RIP homotypic interaction motif; TAT, transactivator; TIR, Toll/interleukin-1 receptor; TNF, tumour necrosis factor; TNFR1, tumour necrosis factor receptor 1; vICA, viral inhibitor of caspase activation; VZV, varicella zoster virus; ZBP1, Z-DNA-binding protein 1.

References

1 Bedoui, S., Herold, M.J. and Strasser, A. (2020) Emerging connectivity of programmed cell death pathways and its physiological implications. *Nat. Rev. Mol. Cell Biol.* **21**, 678–695 https://doi.org/10.1038/s41580-020-0270-8

2 Christgen, S., Tweedell, R.E. and Kanneganti, T.D. (2021) Programming inflammatory cell death for therapy. *Pharmacol. Ther.* 108010 https://doi.org/10.1016/j.pharmthera.2021.108010

3 Petrie, E.J., Czabotar, P.E. and Murphy, J.M. (2019) The structural basis of necroptotic cell death signaling. *Trends Biochem. Sci.* **44**, 53–63 https://doi.org/10.1016/j.tibs.2018.11.002

4 Cho, Y.S., Challa, S., Moquin, D., Genga, R., Ray, T.D., Guildford, M. et al. (2009) Phosphorylation-driven assembly of the RIP1–RIP3 complex regulates programmed necrosis and virus-induced inflammation. *Cell* **137**, 1112–1123 https://doi.org/10.1016/j.cell.2009.05.037
5 Upton, J.W., Kaiser, W.J. and Mocarski, E.S. (2010) Virus inhibition of RIP3-dependent necrosis. *Cell Host Microbe* **7**, 302–313 https://doi.org/10.1016/j.chom.2010.03.006
6 He, S., Liang, Y., Shao, F. and Wang, X. (2011) Toll-like receptors activate programmed necrosis in macrophages through a receptor-interacting kinase-3-mediated pathway. *Proc. Natl Acad. Sci. U.S.A.* **108**, 20054–20059 https://doi.org/10.1073/pnas.1116302108
7 Upton, J.W., Kaiser, W.J. and Mocarski, E.S. (2012) DAI/ZBP1/DLM-1 complexes with RIP3 to mediate virus-induced programmed necrosis that is targeted by murine cytomegalovirus vIRA. *Cell Host Microbe* **11**, 290–297 https://doi.org/10.1016/j.chom.2012.01.016
8 Kaiser, W.J., Sridharan, H., Huang, C., Mandal, P., Upton, J.W., Gough, P.J. et al. (2013) Toll-like receptor 3-mediated necrosis via TRIF, RIP3, and MLKL. *J. Biol. Chem.* **288**, 31268–31279 https://doi.org/10.1074/jbc.M113.462341
9 Wu, X., Ma, Y., Zhao, K., Zhang, J., Sun, Y., Li, Y. et al. (2021) The structure of a minimum amyloid fibril core formed by necroptosis-mediating RHIM of human RIPK3. *Proc. Natl Acad. Sci. U.S.A.* **118**, e2022933118 https://doi.org/10.1073/pnas.2022933118
10 Li, J., McQuade, T., Siemer, A.B., Napetschnig, J., Moriwaki, K., Hsiao, Y.S. et al. (2012) The RIP1/RIP3 necrosome forms a functional amyloid signaling complex required for programmed necrosis. *Cell* **150**, 339–350 https://doi.org/10.1016/j.cell.2012.06.019
11 Pham, C.L., Kwan, A.H. and Sunde, M. (2014) Functional amyloid: widespread in nature, diverse in purpose. *Essays Biochem.* **56**, 207–219 https://doi.org/10.1042/bse0560207
12 Mompeán, M., Li, W., Li, J., Laage, S., Siemer, A.B., Bozkurt, G. et al. (2018) The structure of the necrosome RIPK1–RIPK3 core, a human hetero-amyloid signaling complex. *Cell* **173**, 1244–1253 https://doi.org/10.1016/j.cell.2018.03.032
13 Degterev, A., Ofengeim, D. and Yuan, J. (2019) Targeting RIPK1 for the treatment of human diseases. *Proc. Natl Acad. Sci. U.S.A.* **116**, 9714–9722 https://doi.org/10.1073/pnas.1901179116
14 Moerke, C., Jaco, I., Dewitz, C., Müller, T., Jacobsen, A.V., Gautheron, J. et al. (2019) The anticonvulsive Phenhydan® suppresses extrinsic cell death. *Cell Death Differ.* **26**, 1631–1645 https://doi.org/10.1038/s41418-018-0232-2
15 Riebeling, T., Jamal, K., Wilson, R., Kolbrink, B., von Samson-Himmelstjerna, F.A., Moerke, C. et al. (2021) Primidone blocks RIPK1-driven cell death and inflammation. *Cell Death Differ.* **28**, 1610–1626 https://doi.org/10.1038/s41418-020-00690-y
16 Upton, J.W., Kaiser, W.J. and Mocarski, E.S. (2008) Cytomegalovirus M45 cell death suppression requires receptor-interacting protein (RIP) homotypic interaction motif (RHIM)-dependent interaction with RIP1. *J. Biol. Chem.* **283**, 16966–16970 https://doi.org/10.1074/jbc.C800051200
17 Jiao, H., Wachsmuth, L., Kumari, S., Schwarzer, R., Lin, J., Eren, R.O. et al. (2020) Z-nucleic-acid sensing triggers ZBP1-dependent necroptosis and inflammation. *Nature* **580**, 391–395 https://doi.org/10.1038/s41586-020-2129-8
18 Omoto, S., Guo, H., Talekar, G.R., Roback, L., Kaiser, W.J. and Mocarski, E.S. (2015) Suppression of RIP3-dependent necroptosis by human cytomegalovirus. *J. Biol. Chem.* **290**, 11635–11648 https://doi.org/10.1074/jbc.M115.646042
19 Mandal, P., Nagrani, L.N., Hernandez, L., McCormick, A.L., Dillon, C.P., Koehler, H.S. et al. (2021) Multiple autonomous cell death suppression strategies ensure cytomegalovirus fitness. *Viruses* **13**, 1707 https://doi.org/10.3390/v13091707
20 Mocarski, E.S., Guo, H. and Kaiser, W.J. (2015) Necroptosis: the Trojan horse in cell autonomous antiviral host defense. *Virology* **479–480**, 160–166 https://doi.org/10.1016/j.virol.2015.03.016
21 Hu, H., Wu, X., Wu, G., Nan, N., Zhang, J., Zhu, X. et al. (2021) RIP3-mediated necroptosis is regulated by inter-filament assembly of RIP homotypic interaction motif. *Cell Death Differ.* **28**, 251–266 https://doi.org/10.1038/s41418-020-0598-9
22 Pham, C.L., Shanmugam, N., Strange, M., O'Carroll, A., Brown, J.W., Sierecki, E. et al. (2019) Viral M45 and necroptosis-associated proteins form heteromeric amyloid assemblies. *EMBO Rep.* **20**, e46518 https://doi.org/ 10.15252/embr.201846518
23 Krautwald, S., Dewitz, C., Fändrich, F. and Kunzendorf, U. (2016) Inhibition of regulated cell death by cell-penetrating peptides. *Cell Mol. Life Sci.* **73**, 2269–2284 https://doi.org/10.1007/s00018-016-2200-7
24 Zaidi, N., Herrmann, T., Baechle, D., Schleicher, S., Gogel, J., Driessen, C. et al. (2007) A new approach for distinguishing cathepsin E and D activity in antigen-processing organelles. *FEBS J.* **274**, 3138–3149 https://doi.org/10.1111/j.1742-4658.2007.05846.x
25 Jores, T., Klinger, A., Groß, L.E., Kawano, S., Flinner, N., Duchardt-Ferner, E. et al. (2016) Characterization of the targeting signal in mitochondrial β-barrel proteins. *Nat. Commun.* **7**, 12036 https://doi.org/10.1038/ncomms12036
26 Zhang, D.W., Shao, J., Lin, J., Zhang, N., Lu, B.J., Lin, S.C. et al. (2009) RIP3, an energy metabolism regulator that switches TNF-induced cell death from apoptosis to necrosis. *Science* **325**, 332–336 https://doi.org/10.1126/science.1172308
27 Tweedell, R.E., Malireddi, R.K.S. and Kanneganti, T.D. (2020) A comprehensive guide to studying inflammasome activation and cell death. *Nat. Protoc.* **15**, 3284–3333 https://doi.org/10.1038/s41596-020-0374-9
28 Müller, T., Dewitz, C., Schmitz, J., Schröder, A.S., Bräsen, J.H., Stockwell, B.R. et al. (2017) Necroptosis and ferroptosis are alternative cell death pathways that operate in acute kidney failure. *Cell Mol. Life Sci.* **74**, 3631–3645 https://doi.org/10.1007/s00018-017-2547-4
29 Schwamborn, M., Schumacher, J., Sibold, J., Teiwes, N.K. and Steinem, C. (2017) Monitoring ATPase induced pH changes in single proteoliposomes with the lipid-coupled fluorophore Oregon Green 488. *Analyst* **142**, 2670–2677 https://doi.org/10.1039/C7AN00215G
30 Kolbrink, B., Riebeling, T., Kunzendorf, U. and Krautwald, S. (2020) Plasma membrane pores drive inflammatory cell death. *Front. Cell Dev. Biol.* **8**, 817 https://doi.org/10.3389/fcell.2020.00817
31 Shanmugam, N., Baker, M., Sanz-Hernandez, M., Sierecki, E., Gambin, Y., Steain, M. et al. (2021) Herpes simplex virus encoded ICP6 protein forms functional amyloid assemblies with necroptosis-associated host proteins. *Biophys. Chem.* **269**, 106524 https://doi.org/10.1016/j.bpc.2020.106524
32 Guo, H., Omoto, S., Harris, P.A., Finger, J.N., Bertin, J., Gough, P.J. et al. (2015) Herpes simplex virus suppresses necroptosis in human cells. *Cell Host Microbe* **17**, 243–251 https://doi.org/10.1016/j.chom.2015.01.003
33 Krautwald, S., Ziegler, E., Rölver, L., Linkermann, A., Keyser, K.A., Steen, P. et al. (2010) Effective blockage of both the extrinsic and intrinsic pathways of apoptosis in mice by TAT-crmA. *J. Biol. Chem.* **285**, 19997–20005 https://doi.org/10.1074/jbc.M110.122127
34 Krautwald, S., Ziegler, E., Tiede, K., Pust, R. and Kunzendorf, U. (2004) Transduction of the TAT-FLIP fusion protein results in transient resistance to Fas-induced apoptosis in vivo. *J. Biol. Chem.* **279**, 44005–44011 https://doi.org/10.1074/jbc.M401327200
35 Green, M., Ishino, M. and Loewenstein, P.M. (1989) Mutational analysis of HIV-1 Tat minimal domain peptides: identification of trans-dominant mutants that suppress HIV-LTR-driven gene expression. *Cell* **58**, 215–223 https://doi.org/10.1016/0092-8674(89)90417-0

Biochemical Journal (2022) **479** 259–272
https://doi.org/10.1042/BCJ20210677

36 Mompeán, M., Bozkurt, G. and Wu, H. (2019) Mimicry by a viral RHIM. *EMBO Rep.* **20**, e47433 https://doi.org/10.15252/embr.201847433
37 Huang, Z., Wu, S.Q., Liang, Y., Zhou, X., Chen, W., Li, L. et al. (2015) RIP1/RIP3 binding to HSV-1 ICP6 initiates necroptosis to restrict virus propagation in mice. *Cell Host Microbe* **17**, 229–242 https://doi.org/10.1016/j.chom.2015.01.002
38 Rashidi, M., Wicks, I.P. and Vince, J.E. (2020) Inflammasomes and cell death: common pathways in microparticle diseases. *Trends Mol. Med.* **26**, 1003–1020 https://doi.org/10.1016/j.molmed.2020.06.005
39 Verbeek, S.F., Awasthi, N., Teiwes, N.K., Mey, I., Hub, J.S. and Janshoff, A. (2021) How arginine derivatives alter the stability of lipid membranes: dissecting the roles of side chains, backbone and termini. *Eur. Biophys. J.* **50**, 127–142 https://doi.org/10.1007/s00249-021-01503-x
40 Brune, W. and Andoniou, C.E. (2017) Die another day: inhibition of cell death pathways by cytomegalovirus. *Viruses* **9**, 249 https://doi.org/10.3390/v9090249
41 Hüttmann, J., Krause, E., Schommartz, T. and Brune, W. (2015) Functional comparison of molluscum contagiosum virus vFLIP MC159 with murine cytomegalovirus M36/vICA and M45/vIRA proteins. *J. Virol.* **90**, 2895–2905 https://doi.org/10.1128/JVI.02729-15
42 Daskalov, A., Habenstein, B., Sabaté, R., Berbon, M., Martinez, D., Chaignepain, S. et al. (2016) Identification of a novel cell death-inducing domain reveals that fungal amyloid-controlled programmed cell death is related to necroptosis. *Proc. Natl Acad. Sci. U.S.A.* **113**, 2720–2725 https://doi.org/10.1073/pnas.1522361113
43 Kounatidis, I. and Ligoxygakis, P. (2012) Drosophila as a model system to unravel the layers of innate immunity to infection. *Open Biol.* **2**, 120075 https://doi.org/10.1098/rsob.120075
44 Baker, M., Shanmugam, N., Pham, C.L.L., Strange, M., Steain, M. and Sunde, M. (2020) RHIM-based protein:protein interactions in microbial defence against programmed cell death by necroptosis. *Semin. Cell Dev. Biol.* **99**, 86–95 https://doi.org/10.1016/j.semcdb.2018.05.004
45 Steain, M., Baker, M., Pham, C.L.L., Shanmugam, N., Gambin, Y., Sierecki, E. et al. (2020) Varicella zoster virus encodes a viral decoy RHIM to inhibit cell death. *PLoS Pathog.* **16**, e1008473 https://doi.org/10.1371/journal.ppat.1008473
46 Kim, D.H. and Frangos, J.A. (2008) Effects of amyloid beta-peptides on the lysis tension of lipid bilayer vesicles containing oxysterols. *Biophys. J.* **95**, 620–628 https://doi.org/10.1529/biophysj.107.114983
47 Breydo, L. and Uversky, V.N. (2015) Structural, morphological, and functional diversity of amyloid oligomers. *FEBS Lett.* **589**, 2640–2648 https://doi.org/10.1016/j.febslet.2015.07.013
48 Otzen, D. and Riek, R. (2019) Functional amyloids. *Cold Spring Harb. Perspect. Biol.* **11**, a033860 https://doi.org/10.1101/cshperspect.a033860
49 Liu, Y., Dai, Y., Li, Q., Chen, C., Chen, H., Song, Y. et al. (2020) Beta-amyloid activates NLRP3 inflammasome via TLR4 in mouse microglia. *Neurosci Lett.* **736**, 135279 https://doi.org/10.1016/j.neulet.2020.135279
50 Vanmeerbeek, I., Sprooten, J., De Ruysscher, D., Tejpar, S., Vandenberghe, P., Fucikova, J. et al. (2020) Trial watch: chemotherapy-induced immunogenic cell death in immuno-oncology. *Oncoimmunology* **9**, 1703449 https://doi.org/10.1080/2162402X.2019.1703449
51 Galluzzi, L., Buqué, A., Kepp, O., Zitvogel, L. and Kroemer, G. (2017) Immunogenic cell death in cancer and infectious disease. *Nat. Rev. Immunol.* **17**, 97–111 https://doi.org/10.1038/nri.2016.107